Melt Rheological Investigation of Polylactide-Nanographite Platelets Biopolymer Composites

Esmaeil Narimissa, Rahul K Gupta*, Nhol Kao, Hyoung J. Choi^, Margaret Jollands and Sati N. Bhattacharya

Rheology and Materials Processing Centre (RMPC), School of Civil, Environmental and Chemical Engineering, RMIT University, 124 La Trobe St, Melbourne, Vic 3000, Australia

^Department of Polymer Science and Engineering, Inha University, Incheon, 402-751 Korea

**Corresponding Author: E-mail: rahul.gupta@rmit.edu.au, Phone: + (61 3) 9925 8347*

ABSTRACT

The current study is an analytical investigation of processability of biopolymer-carbon based nanofiller composites primarily through rheological investigation of samples. The composites were fabricated via dry mixing and melt-blending of biodegradable polylactide (PLA) and nano graphite platelets (NGP) in a Brabender twin screw extruder. A range of different nanofiller contents (1, 3, 5, 7 and 10 wt%) were studied for NGP containing composites. The morphology was studied with X-ray Diffraction (XRD) and Transmission Electron Microscopy (TEM) techniques and showed poor dispersion, with agglomerates, tactoids and exfoliated layers present. Mechanical properties showed an optimum at 3 wt% filler. Results showed that the composites exhibited higher elastic and viscous moduli than neat PLA. The rheological percolation threshold predicted by changes in slope (α) as well as liquid-solid transition theory of samples was found around 3 wt% through the change from liquid-like behaviour to pseudo-solid-like behaviour at terminal region during dynamic oscillatory measurements. NGP nanofillers were found to enhance the viscoelastic and mechanical properties of PLA at low concentrations; however, an efficient dispersion of nanofillers within polymer by melt intercalation method of mixing was not achieved.

Abbreviation

PLA: Polylactide; TEM: Transmission Electron Microscopy; XRD: X-ray Diffraction; CSR: Critical Strain Rate, LST: Liquid-Solid-Transition, T_{gel}: Gelation Temperature

1. Introduction

In the production of bioplastics, biodegradable natural polymers extracted from renewable resources such as polylactide (PLA), polycaprolactone (PCL), cellulose and starch are considered a more suitable alternative than petroleum-derived synthetic plastics. The degradation of these polymers by microorganisms generates nontoxic components in the environment reducing world-wide dependence on fossil fuels [1, 2]. Disposal of non-biodegradable polymers and their composites through incineration on the other hand, may produce toxic gases and contribute to global pollution [3]. Research in the field of bionanocomposites can contribute to the efficiency of recycling waste management and green house emissions. The Benign properties of PLA towards the environment and its production from renewable resources make it a strong candidate as a substitute for petroleum based polymers.

PLA is a biodegradable thermoplastic polyester with linear aliphatic monomers, polymerized from lactic acid derived from fermentation of cornstarch [2]. Despite a number of PLA's promising properties (i.e. biocompatibility, thermal plasticity and mechanical properties) it has failed to show similar satisfactory outcomes in its gas barrier properties, impact factor, and heat distortion temperature in different applications [4, 5]. Insufficient thermal, mechanical, barrier and flame retardant properties of PLA have limited its application [6]. For example, automotive industry applications require material properties, where PLA grades are deficient in high durability, tight tolerances and efficient impact performance. The control of crystallinity of PLA through the addition of nanosized particles could lead to improvements in PLA properties such as heat deflection temperature, overall strength, chemical resistance, and stiffness [7]. The most popular nano-reinforcement in PLA studies to date is layered-silicate clay. This is due to the nanofiller's low cost, availability and satisfactory enhancements brought into mechanical, barrier and thermal properties of neat PLA, in addition to its acting as a nucleating agent to improve the crystallinity of PLA [8, 9].

Melt intercalation is the main process for fabrication of PLA bionanocomposites, due to its simplicity and economic viability [10, 11]. This process has been shown to produce interrelated nanocomposites with improved properties such as stiffness, thermal stability, fire retardancy and lower barrier permeability [9, 12]. Exfoliation of nanofillers in PLA nanocomposites has been demonstrated via in-situ polymerization of lactic acid monomers as well as solvent casting technique [13].

Graphene is a monolayer of sp^2-hybridized carbon atoms arranged in a two-dimensional lattice, which has been studied extensively due to its extraordinary thermal, mechanical and electrical properties [14-16]. Nanocomposites have been amongst the most promising areas of application of graphene based compounds [17]. Micromechanical exfoliation of graphite, growth by chemical vapor deposition and growth on crystalline silicon carbide are the main approaches to producing defect free pristine graphene with exceptional physical properties [14, 18]. However, these techniques do not produce sufficient quantities of graphene required for industrial-scale fabrication of nanocomposites [19]. Thus, producing nanocomposites using graphene-based compounds through the precursors of graphene (such as graphite oxide (GO) and nanographite platelets (NGPs) is a suitable alternative method [17].

Intercalation of graphite by a mixture of nitric and sulphuric acid can produce higher-stage graphite-intercalated compounds (GIC) that can be exfoliated via microwave treatment or rapid heating of dried down generating expanded graphite (EG) [20, 21]. GICs and GOs can be subsequently utilized as precursor materials to produce scalable NGPs (monolayer carbon sheets or few-layer platelets with heteroatoms). NGPs contain a platelet structure and low price of clay, possess electrical and thermal properties of carbon nanotubes (CNTs) and have the potential to improve the crystallization behaviour of PLA. Furthermore, due to their length and thickness, the entanglement of CNTs and carbon nanofibres (CNFs) are compatible with NGPs, which may contribute in the

reduction of agglomeration. In addition, the electrical conductivity of NGPs is close to the electrical conductivity of copper, while also having a quarter of its density and fifty times higher mechanical strength than steel [22, 23]. In terms of crystallization, research has shown that NGPs can induce the nucleation of β-form crystals In polypropylene (PP), which are superior to α-form [24].

The main objective of the current study was to investigate the interfacial compatibility and interactions between polylactide chains and nanographite platelets for the purpose of fabricating biodegradable PLA/NGP nanocomposites via dry mixing and melt blending processes. In order to achieve this goal, melt rheological characterization of the samples was followed by the modelling of the results through utilization of eminent mathematical steady and dynamic rheological models of viscoelasticity. The steady shear rheology of the samples was investigated by means of Carreau-Yasuda model as well as the application of Cox-Merz relation while time-temperature superposition and slope α analysis of the percolation threshold were applied to study the dynamic shear rheological behaviours of samples. Additionally, a comprehensive investigation based on liquid-solid transition theory, proposed by Winter and Chambon (1986), was also carried out to study the percolation threshold and gelation properties of the composites. Furthermore, the authors have already performed detailed investigations of the thermal, morphological and mechanical properties of the samples [25-27].

2. EXPERIMENTAL

2.1 Materials

Poly (L,L-lactide)- (PLA) was supplied by NatureWorks LLC and the grade of PLA used was 3051D with melt index and specific gravity of 10-30g/10min and 1.24 respectively. Nanographite platelets (NGPs) were supplied by XG Sciences, Inc US Michigan and the grade of NGP used for

this study was "M" with characteristics: average thickness of approximately 6 - 8 nanometers and a typical surface area of 120 to 150 m^2/g. According to the material data sheet, Grade M (xGnp-M) is available with average particle diameters of 5, 15 or 25 microns.

2.2 Processing

Drying of PLA to less than 250 ppm is a necessary first step prior to the processing phase. Thus, PLA pellets used in this study were first dried in a fan dryer at a temperature of 50 ^{o}C for 7 days earlier than the melt blending process.

PLA pellets and nanographite platelets (NGP) were dry mixed in the desired composition before melt blending in 700g batches. Table 1 shows the compositions (nominal wt%) and the codes of neat PLA and PLA/NGP samples (hereafter, samples are referred to according to their sample codes).

Samples were melt-blended in a Brabender Twin Screw extruder. The speed and temperature of the extruder were set at 180 ^{o}C and 40 RPM, as too high or too low extrusion temperatures or speed may result in thermal degradation and/or insufficient shear for proper mixing of nanocomposites. Subsequently, the extruded composites were pelletized and then stored in a vacuum oven at 50 ^{o}C before further processing.

Dried pellets were compression moulded into 2 mm thick circular plaque with 20 mm diameter specimens. The compression moulding temperature was 180 ^{o}C and the compression force was kept at 80 kN for 5 minutes. Cooling water was used to cool the moulding press from 180 to 50 ^{o}C.

Samples were stored in a vacuum oven at 50 ^{o}C. Portable desiccators containing silica gels were used to carry the samples from the vacuum oven to characterization instruments.

2.3 Characterization

2.3.1 Rheological measurements

The dynamic and steady shear measurements were performed through an Advanced Rheometrics Expansion System (ARES) rheometer (TA Instruments) with parallel plate geometry using 20 mm diameter plates. A force transducer with a torque range of 0.2 to 200 gm-cm was applied to all measurements. Dynamic shear measurements were performed by applying time dependent strain of $\gamma(t) = \gamma_0 \sin(\omega t)$ and measuring resultant shear stress of $\tau(t) = \gamma_0[G'(\omega)\sin(\omega t) + G''(\omega)\cos(\omega t)]$ where G' and G" are storage and loss moduli [28]. The samples were initially 2 mm thick, but were then reduced to 1.65 mm through gap size setting prior to the commencement of the measurements. The temperature range of dynamic measurements was 170-200 ^{0}C and the steady shear measurements were performed at 180 ^{0}C, consistent with the application of the typical processing temperature of PLA. A strain amplitude of 5% was applied to the PLA in order to avoid nonlinear response at elevated temperatures or low frequency regions [28]. Dynamic strain sweep tests were executed to determine the limits of linear viscoelasticity at fixed frequencies.

2.3.2 Morphological Evaluations (XRD and TEM)

Wide angle X-ray (WAXS), Rikaku X-ray diffractometer (the wavelength of 0.154 nm) with 40 kV accelerating voltage and 40 mA current for recording data within a range of 2θ =10~80^o were utilized in the current study. Transmission electron microscopy (TEM) images were obtained with a Phillips CM200 operated at an acceleration voltage of 120kV. The samples were ultramicrotomed using a RMC ultramicrotome with CR-X Cryosection at -160 ^{o}C. TEM micrographs were printed on A4 sheets and the filler dimensions were measured and analyzed according to the image magnification of 0.2 μm.

2.3.3 Mechanical Testing Measurements

Tensile testing measurements were performed using an Instron 4467 Universal testing machine in accordance to ASTM D638M norm, at speed rate of 1mm/min using a distance of 115 mm between grips and the extensometer was set at 50 mm separation. Measurements were carried out at ambient temperature.

3. RESULTS AND DISCUSSION

3.1 Morphological Properties

The crystalline structures and the dispersion of nanofillers were investigated using XRD and TEM in the current study. Figure 1 illustrates the diffractograms recorded for the samples at ambient condition. The presence of a scattered intensity distribution with a broad maximum around 2θ~16.5^{o} in composites, indicates a semi crystalline structure of PLA. The diffractograms also demonstrated an intense peak at 2θ value of ~ 26^{o} assigned to intercalated nanographite platelet layers at a distance of 0.341 nm, which has been detected at similar 2θ value for graphite sheets in earlier studies [29-31]. The same d-spacing of graphite layers was found in all composites and suggests that the melt-blending process did not separate the graphite layers. Fig. 2 shows TEM images of composites at 0.2 μm magnification obtained via direct dosing and melt blending of nanofillers into PLA. A hybrid morphology of agglomerated and intercalated layers of graphite sheets were evident in the micrographs (Fig. 2 a, f) .The lengths of these nanolayers were several hundreds of nanometers. In addition, tactoids were present in 3-10 wt% NGP composites, which suggest that the sharp peaks at 2θ~26^{o} may be a consequence of tactoids or intercalated NGP layers. The TEM micrographs also illustrated some perpendicular orientation of platelets (~20-50 nm thickness) to images' surface area (2.1 μm X 2.1 μm).

Overall, the morphological characterization of the current study demonstrated tactoid and agglomerate formation in coexistence with limited intercalation and partial individualization. Indeed, the majority of the graphite layers were still present in aggregate structure, which may have been due to the strong bond between the graphite sheets that kept them interlinked with one another and only allowed partial exfoliation of NGP fillers [32]. Unlike nanofillers, such as organically

modified layered silicate (OMLS), melt blending and dry mixing processes may not be capable of efficient dispersion and individualization of graphite layers. Thus, through the mixing process, PLA/NGP samples may only be identified as hybrid nano/micro-composites and not nanocomposites.

3.2 Mechanical Properties

Fig 3, illustrates the Young's modulus and elongation at break of the samples as a function of filler content. The incorporation of NGP into PLA significantly increased the Young's modulus. The sample with 3 wt% NGP content had the highest modulus, 135% higher than the base polymer. The optimum content of around 3 wt% nanofiller is consistent with the mechanical percolation threshold reported for platey nanocomposites [33]. Although the morphological characterization showed poor dispersion of nanofiller in the polymer matrix, the enhancement in elastic modulus can be attributed to the partial intercalation of polymer chains in NGP galleries resulting in reinforcement of the system [34]. A gradual decrease in modulus was found for filler contents of 5-10 wt%, which may be assigned to the inability of filler to intercalate above the percolation threshold. This may also be due to the tendency of NGP particles to aggregate at higher loadings. As Fig. 3 illustrates, the addition of NGP resulted in a decrease in elongation at break for the composites. Thellen and colleagues [35] reported that the addition of nanofillers to plastics typically decreases the composites' elongation considerably and increases their embrittelment. The mechanical properties of the samples in the current study have already been reported by the authors [26].

3.3 Dynamic Shear Rheology

3.3.1 Dynamic strain sweep test

Dynamic strain sweep tests were conducted at 180 ^{o}C and at a constant frequency of 1(i.e. for 0, 1, 3% NGP) and 5 rad/s (i.e. for 5, 7, 10% NGP). Between the two rheological parameters, storage

modulus (G') and loss modulus (G"), the storage modulus is considered the most sensitive to changes in microstructure during the study. The critical strains were measured as the onset of drop in G' while increasing strain, which marked the onset of alignment of nanographite platelets at lower strain amplitudes. The critical strain values demonstrated the onset of non-linear viscoelasticity. Fig. 4 shows the relationship between storage modulus (G') and strain. The linear region of each curve depicts linear viscoelastic behaviour of that particular sample. The limit of linearity for the neat PLA and composites are shown in Table 2. For neat PLA and PLA01 no significant change of storage modulus (G') with increasing strain amplitude was found. PLA03 sample showed linear viscoelasticity region up to 25% strain, whereas PLA05, PLA07, and PLA10 composites exhibited highly pronounced nonlinear behaviour, where onset of the G' drop occurred at critical strains less than 2%. The limit of linearity of viscoelastic region tended towards low strains amplitudes at higher NGP concentrations (Table 2).

As a result of the strain exposure of the samples, the neat PLA showed its inherent viscoelastic property while the composites became hard enough to move with shear. However, PLA01 followed a similar behaviour to the neat PLA sample. It is possible that these solid-like behaviors of composites (>1 wt% NGP content) are due to the interaction between the PLA and NGP particles. At sufficiently high strains, strain concentration occurring in the interparticle regions may have led to the perturbation of the entangled bulk matrix structure and the mesostructure of the material could have started to respond according to the deformation [36]. Since the strain applied in the linear region to the samples was not high enough to unrest the mesostructure of the material's equilibrium state, it remained in the quiescent state and the imposed deformation or strain was absorbed by the material as a result [37]. During the high shear process, the mesostructure of the material began to align in the direction of the shear flow. Krishnamoorti et al. (2001) described these alignments as similar to that observed in crystalline polymers and block co-polymers.

3.3.2 Dynamic frequency sweep test

The Dynamic frequency sweep (DFS) tests were conducted at strains close to the critical strain values of samples. Since the rheological properties of polymer melts depend highly on the temperature, the time-temperature superposition principle was applied to produce the master curves with the reference temperature of 180 ^{0}C. For thermo-rheological materials, bi-logarithmic plots of loss and storage modulus, as well as complex viscosity as a function of frequency can be superimposed by horizontal shifts $\log(a_T)$ and vertical shifts $\log(b_T)$ versus $\log(\omega_T)$ axis [38], Where T_{ref} is the reference temperature:

$$b_T G'(a_T\omega, T_{ref}) = b_T G'(\omega, T)$$
$$b_T G''(a_T\omega, T_{ref}) = b_T G''(\omega, T)$$
$$(b_T / a_T)\left|\eta^*\right|(a_T\omega, T_{ref}) = \left|\eta^*\right|(\omega, T)$$

RSI Orchestrator software (Version 6.5.8, developed by Rheometric Scientific) was employed to plot the master curves and the steady shear viscosity measurements were conducted using parallel plate geometry with the sample thickness of 1.65 mm and plate diameter of 20 mm. Fig. 5 illustrates the bi-logarithmic master curves of the storage modulus (G') and loss modulus (G") as a function of frequency $(a_T\omega)$ of neat PLA and PLA/NGP composites. Both G' and G" of samples increased monotonically at all frequencies. Homopolymer-like terminal flow behaviour was expected to be exhibited by neat polymer samples at low frequency region [28]. As shown in Fig. 5, terminal behaviour $\left(G'(\omega) \propto \omega^2, G''(\omega) \propto \omega^1\right)$ was observed at the lower frequency (terminal) region $(a_T\omega < 10)$ of the neat PLA and PLA01 samples. At higher NGP content (3-10 wt% NGP), pseudo-solid like behaviors $\left(G'(\omega), G''(\omega) \propto \omega^0\right)$ were observed at terminal regions, which can mainly be applied to homopolymers that behave as Newtonian fluids. For composites, the slope of moduli at low frequencies characterizes their quiescent nature [39]. Storage modulus of PLA01 and PLA03 composites behaved similarly to neat PLA. At low frequencies, there was an increase in G' when

the concentration of NGP was increased from 0 to 3 wt%, while, at higher frequencies $(a_T\omega > 10\,rad/s)$ storage modulus of those composites attained similar values as neat PLA. PLA05, PLA07 and PLA10 composites were comparable in behaviour, however, at higher frequency regions, G' of all samples coincided with each other. Loss moduli of samples at measured frequencies $(a_T\omega \approx 0.01-100\,rad/s)$ were distinctively higher than their corresponding storage moduli and showed monotonic increases over this frequency range. Nevertheless, at high frequency region $(a_T\omega \approx 100\,rad/s)$ G' and G" of all samples coincided and appeared to cross over (Fig. 5). At frequency regions $(a_T\omega \approx 10-100\,rad/s)$, less increase in both G' and G" was observed which could be attributed to the alignment of anisotropic NGP platelets or stacks of platelets in the direction of the flow. As a result of this alignment, less moduli enhancement was shown in the results.

The liquid-like (terminal) behaviour observed in neat PLA gradually changed to pseudo-solid-like behaviour at 3 wt% NGP loading (PLA03). The exhibition of pseudo-solid-like behaviour at high filler content (>3 wt% NGP) composites may have been due to the prevented relaxation caused by high geometric constraints or physical jamming of the agglomerated NGP layers and filler's tactoid formation. Moreover, the lower slope of storage modulus as well as their corresponding higher absolute values of both moduli for higher filler content composites can be a result of the formation of spatially-linked structure under molten state of processing [40].

Fig. 6 illustrates the master curves of dynamic complex viscosity of the samples. Neat PLA, PLA01 and PLA03 exhibited Newtonian like behaviour at low frequency regions $(a_T\omega < 10)$. The deviation from Newtonian like behaviour to shear thinning behaviour occurred at PLA03 and became more accentuated for PLA05, PLA07 and PLA10. It was also clear that the zero complex viscosity of samples enhanced as the amount of filler content increased. This result may be due to the elevated limitation of polymer chain flow in molten state caused by addition of nanofillers to the polymer matrix. Okomoto et al. (2000) and Sinha Ray (2003) reported similar shear thinning behaviour of platy nanofillers like clay in the rapid shear flow. This characteristic has been attributed in literature

to the shear-induced alignment of the dispersed clay particles in polymer matrix and its strong dependence on the shear rate in dynamic measurements [41].

At higher frequency regions $(a_T\omega > 10\,rad/s)$, all samples exhibited shear thinning behaviour. This can be a result of the alignment of NGP layers in the direction of shear at high frequency regions, where the filler contents have small effect on the complex viscosity of composites and the relaxation mechanism was mainly governed by the polymer matrix. This is unlike the lower frequency regions, where the relaxation mechanism was dominated by particle-particle interactions inside the percolated network of NGP layers [42]. Furthermore, the applicability of the time-temperature superposition principle for PLA/NGP samples is a significant indication of thermo-rheological simplicity of these composites upon which it exhibits the predictability of these materials' rheological characteristics when subjected to non-stationary and non-uniform temperature fields [43, 44].

Bhattacharya [45] defined the percolation threshold for filler loading as the level beyond which the formation of a three-dimensional percolated network is established and the filler-filler interactions become significant. Thus, the evaluation of the percolation threshold can be performed during the linear viscoelastic regime when a sudden change of behaviour (slope (α)) occurs from liquid-like response to solid-like response [46-48]. This transformation could be due to the fact that as the filler content increases, the frequency dependence of the composites decreases and the moduli tend to become ω-independent at the terminal region. Consequently, such end-result could cause the exhibition of a solid-like behaviour at low frequencies, indicating the formation of percolation networks within the polymeric matrix. The slope (α) ,i.e. slope of monotonic increase of moduli as a function of frequency at terminal regions, of storage modulus versus frequency of all samples was manually measured at low frequency range ($0.01 > \omega > 1$) (the results are shown in Table 3). Results found the highest value of 1.9 for neat polymer, with a decrease for NGP loadings of 1-10 wt%. Fig. 7 demonstrates the slope (α) of samples versus their NGP contents. The change in slope of the moving average trendline with period of two marks the percolation threshold region of PLA/NGP composites about 3 wt% filler content. This threshold corresponds to the formation of a three-

dimensional network structure, whereby NGP platelets act as physical cross-linkers, hence forming a mesostructure with enhanced interactions [45]. Beyond 3 wt% NGP concentration, (i.e. PLA05 and PLA07) composites showed pseudo-solid like behaviour when G' became nearly independent of frequency (ω). PLA10 demonstrated solid behaviour with slope (α) value of zero; thus, it was not considered for determining the percolation threshold region.

Overall, dynamic rheological properties of samples including complex viscosity, storage and loss moduli confirmed that the gradual changes from liquid-like behaviour in neat PLA, PLA01 and PLA03 samples to pseudo-solid like behaviour in PLA05-PLA10 samples were evident. Therefore, it can be concluded that due to this change in samples' behaviour, percolation threshold region was attained.

3.4 Steady Shear Rheology

Fig. 8 demonstrates the dependence of steady shear viscosity (η) on shear rate as measured at 180 ^{o}C. The zero-shear viscosity of neat PLA and PLA01 did not show any marked differences, however, PLA03's zero-shear viscosity was almost 30% higher than neat PLA. Elevations in shear viscosity to 65%, 110% and 220% in PLA05, PLA07 and PLA10 composites were found (Table 4). The intersection between the Newtonian region at low shear rate and the shear-thinning region (power law behaviour) occurred at the critical shear rate (CSR). The inverse of the CSR is approximately equivalent to the characteristic time of the samples, which is the longest relaxation time required for elastic structure [34]. Although non-Newtonian shear thinning behaviour was observed in all samples, it started at drastically lower shear rates as the NGP content of composites increased above 3 wt%. The shear thinning nature of PLA/NGP indicates that PLA/NGP composites can efficiently undergo melt processing [49]. Indeed, for PLA07 and PLA10 samples the exhibition of low shear viscosity plateau was not clear enough. Furthermore, the observed enhancement in shear thinning behaviour at very low shear rates for higher filler content (5-10 wt%) composites might also be a sign of polymer imprisonment between NGP particles and layers, by which a larger effective strain rate could have been experienced [50, 51]. In other words, it

simply exhibited the enhanced energy dissipation in the presence of solid particles, and the smaller particle interaction at lower filler content (1-3 wt%) regimes may be the reason why their viscosities are similar to neat PLA system. Similar observations for polymer-clay nanocomposites have previously been reported in the literature [49, 52, 53]. This noteworthy enhancement in zero-shear viscosity may be due to tactoid formation and agglomeration of nanographite platelets at higher filler contents, resulting in significant interaction between anisotropic graphite platelets, which initiated a strong dependence of viscosity on NGP loading. Comparable results to dynamic complex viscosity were also observed in terms of steady shear viscosity of samples where the shear viscosity of composites became similar to that of neat PLA at high shear rates. According to Krishnamoorti et al. (2001), this independence of composites' viscosity from NGP loading at high shear rates suggests that filler layers and their tactoids contribute negligibly to the overall viscosity due to the ability of NGP layers to become aligned and reorientated in the direction of shear flow.

Overall, the finding of different behaviors in shear viscosity of all composites at low shear rates suggests that the strong orientation of filler layers in the flow direction, as well as similar viscosity and shear thinning behaviour of samples at higher shear rates reveal the dominance of shear rheological properties of neat polymeric system.

Due to the complexity of measuring the steady shear viscosity of highly elastic fluids and polymers at high shear rates using conventional rheometers, a simple empiricism known as Cox-Merz relation was used to estimate the shear viscosity of the material. It was almost unfeasible to measure the shear viscosity of polymer melts at shear rates greater than one with basic flow geometries such as parallel plate arrangements [54]. Thus, high frequency oscillatory data were employed to approximate the steady shear viscosity of polymer melts via the following equation 1 [55]:

$$\left[\eta\left(\dot{\gamma}\right)\right]_{\dot{\gamma}=\omega} = \left|\eta^{*}(\omega)\right| = \sqrt{\eta'^{2}(\omega)+\eta''^{2}(\omega)} \quad (1)$$

According to complex viscosity and steady shear viscosity data presented in previous sections of this study (Figs. 6 and 8), the failure of Cox-Merz relation for composites was evident for this system. The difference between steady-state and dynamic data was more apparent at higher filler

contents. Similar discrepancies with Cox-Merz relation were also reported in different polymer nanocomposite studies where anisotropic fillers (i.e. organo-clay) contents were incorporated into polymeric matrix [34]. Furthermore, it was clear that Cox-Merz relation failed for all shear rates, which may have been a result of the ability of shear force to break filler network and also orientation of NGP layers parallel to flow direction compared to that of the dynamic oscillatory state. Moreover, Cox-Merz rule might be only functional for homogenous systems like neat polymers and not heterogeneous systems like composites. Finally, the difference in structure formation due to dynamic oscillatory shear and steady shear measurements could have been another contributing factor in failure of this relation [40].

Measuring shear viscosity at high shear rates is generally a difficult process, and thus, different models have been developed by various researchers to tackle this issue. The Carreau model (1972) is a prominent three-parameter model given in equation 2:

$$\eta = \frac{\eta_o}{\left[1+\lambda\left(\dot{\gamma}\right)^2\right]^{\frac{(1-n)}{2}}} \qquad (2)$$

Where λ (s) is the characteristic or relaxation time, η_0 (Pa.s) is the zero-shear viscosity and n is a dimensionless parameter which determines the slope of shear viscosity versus shear rate in the shear thinning (power law) region (i.e. slope = n - 1 where $0 \leq n < 1$, special case: Newtonian flow, where n = 1 or $n\dot{\gamma} \to 0$). On the other hand, the Carreau-Yasuda model (1979) is a five-parameter model which provides improved fits and is known as the most reliable model estimating zero-shear viscosity of polymer melts [54]. It is shown in equation 3:

$$\frac{\eta-\eta_\infty}{\eta_o-\eta_\infty} = \frac{1}{\left[1+\lambda\left(\dot{\gamma}\right)^a\right]^{\frac{(1-n)}{a}}} \qquad (3)$$

Where parameter *a* improves the depiction of the transition zone between Newtonian flow and shear thinning regions (i.e. $a = 2$ in Carreau model). η_∞, is the shear viscosity at very high shear rates, however, due to its inaccessibility in this study, it was eliminated from equation 3. The modeling parameters were adjusted to calculate the best fit of the experimental results utilizing Microsoft Solver in Excel 2007 software. Fig. 9 compares the model predictions to viscosity data for neat PLA and PLA/NGP composites. The Carreau-Yasuda model shows enhanced predictability to the Carreau model. However, both models present a relatively weaker prediction in PLA03 composite. Both models showed that the degree of shear thinning behaviour remained almost constant from neat PLA to PLA03 composites and reached its maximum at PLA05 sample. At PLA10 sample, the degree of shear thinning behaviour remained considerably higher than neat PLA to PLA03 composites; however, it was close to that of the PLA05 sample. As already mentioned, this improvement in shear thinning behaviour could be due to the change in composite's microstructure from random orientation to a shear induced ordered orientation and consequently the alignment of NGP layers under shear [49, 56, 57]. The calculated values of *a*, *n* and λ are shown in Table 5. The characteristic times (λ) of neat PLA and PLA/NGP composites were obtained from both models. Significant increases in relaxation times began from PLA03 and reached its maximum at PLA10 sample, which is an indication of early termination of pseudo-solid behaviour at lower shear rates and higher rigidity in composites at higher NGP contents. The importance of the value of *a* parameter is still not well understood in polymeric systems and remains as correction factor for transition between Newtonian to shear thinning behaviour in rheological modeling purposes.

Overall, the prediction of the behaviors of samples was moderately similar in both models. They both indicate a transition of steady shear behaviour from PLA03 to PLA05 composites which is in agreement with the dynamic oscillatory analysis of samples where the change in behaviour was exhibited in the slope (α) (Fig. 7). Furthermore, the mechanical analysis of samples confirmed the presence of a percolation threshold at around PLA03 composite (Fig. 3). Hence, it can be concluded

that the rheological percolation threshold of composites lies somewhere in the vicinity of 3 wt% filler content.

3.5 Liquid-solid transition and gelation property evaluations

In order to investigate the relaxation modulus of the samples, the stress-relaxation tests were performed at 180^0C with strain magnitudes within the viscoelastic region of the samples. According to Winter and Chambon [58, 59], the simple relaxation behaviour of the critical gels is followed by a power law relaxation modulus, where, S (gel strength) and n (relaxation exponent) are the characteristics of the critical gel while λ denotes the relaxation time:

$$G(t) = St^{-n} \quad \text{For} \quad \lambda_0 < t < \infty \qquad (4)$$

The power law region is assumed to be extended to infinite time. The longest relaxation time (λ_{max}) diverges to infinity from the liquid region to the liquid-solid transition (LST) region. Beyond the LST, where the material shows solid-like behaviour, the relaxation modulus demonstrates finite values at long times. This finite modulus is called equilibrium modulus (G_e) and has the following mathematical definition:

$$G_e = \lim_{t\to\infty} G(t) \qquad (5)$$

The value of G_e can be estimated from the relaxation modulus plot and is greater than zero only beyond the gel point. The magnitude of the longest relaxation time or the characteristic time (λ_{max}) can be determined at the intersection between G_e and $G(t) = St^{-n}$ which is also the intersection of the power law region and the linear (horizontal) section of the plots [60]:

$$G_e = (St^{-n})_{t=\lambda_{\max}} \Rightarrow \lambda_{\max} = \left(\frac{G_e}{S}\right)^{-1/n} \qquad (6)$$

The storage and loss moduli of a critical gel obey a scaling law with the same exponent n [61]:

$$G'(\omega), G''(\omega) \propto \omega^n \quad \text{Where } 0 < n < 1 \qquad (7)$$

$$G'(\omega)/G''(\omega) = \tan\delta = \tan(n\pi/2) \qquad (8)$$

G' and G" at the gel point are given by the following formula [62], where $G''/G' = (G''/G')_c$ is the value at which the curves intersect in a single point and Γ(n) is the gamma function.

$$G'(\omega) = G''(\omega)/\tan(n\pi/2) = S\omega^n\Gamma(1-n)\cos(n\pi/2) \qquad (9)$$

Therefore:

$$n = \frac{2}{\pi}\tan^{-1}\left(\frac{G''}{G'}\right) \qquad (10)$$

$$S = \frac{G'(\omega)}{\omega^n \cos(n\pi/2)\Gamma(1-n)} \qquad (11)$$

The relaxation exponent (n) is restricted to values between 0 and 1. The value of n reaches zero for Hookean solids and n < 1 is necessary to assure a diverging zero-shear viscosity at the gel point. The relaxation exponent (n) and the gel strength (S) determine the linear viscoelastic behaviours of critical gels (equation 1). The lack of universal values for critical gels' relaxation exponents, results in the existence of n values, where the critical gel is either soft and fragile (n tends to 0 and S is small) or stiff and hard (n tends to 1 and S is large) [62].

Fig. 10 shows the frequency independent values of tan δ versus NGP filler contents (1-10 wt %). A steady decrease in tan δ with increasing NGP filler content was observed at low frequency regions (ω = 1, 0.316 and 0.1 rad/s). The cross point of the curves at low frequency region occurred at filler contents between 5 and 7 wt% and tan δ value of about 11. The relaxation exponent was calculated via equation 10 and resulted in n value of 0.94. Fig. 11 demonstrates the G' and G''/tan (nπ/2) against filler concentration of the samples. No occurrences of crossover points between G' and G'/tan (nπ/2) were observed. The relaxation modulus versus the relaxation time of the samples is shown in Fig. 12. The samples containing NGP fillers less than 3 wt% (neat PLA-PLA03) demonstrated the absence of the equilibrium modulus (G_e) as their λ_{max} values tend to reach zero at high relaxation times. Dealy and Larson (2006) ascribed the long-time limiting value of G(t)

(equilibrium modulus) to cross-link elastomers whereas its absence (G_e=0) is evident in polymer melts [63]. Nevertheless, conspicuous relaxation equilibriums were detected at filler contents 5-10 wt% (PLA05-PLA10) when the curves plateaued at $\lambda \geq \lambda_{max}$. Fig. 13 illustrates the best fits of the power law trend lines (equation 4) for the relaxation modulus versus relaxation time plots at $\lambda \leq \lambda_{max}$ (the power law region). High values of the coefficient of determinations ($R^2 > 0.97$) for all samples suggest that the power law model proposed by Winter and Chambon fits well to the composites.

Table 6 shows the corresponding values of relaxation equilibriums, characteristic times, gamma functions, gel strengths and relaxation exponents of the samples. The presence of G_e and λ_{max} was recorded in PLA05-PLA10 composites only, while neat PLA-PLA03 samples did not show any solid like behaviour at all relaxation times (G_e and λ_{max} = 0). The only distinguished trend was found in the values of λ_{max} which markedly decreased from PLA05-PLA10 samples. However, the calculated values of n and S did not satisfy the ranges proposed by Winter and Chambon (1997).

In a study performed on PVC6, PVC8, Sugimoto (2007) showed that the occurrence of the critical gel is only possible at a certain temperature called the critical gel temperature (T_{gel}) at which the terminal slope of loss and storage moduli becomes independent of frequency. It was shown that over a temperature range of 150-220ºC, such behaviour was only observed at T_{gel} of 190 ºC (PVC8) and 210 ºC (PVC6) in ω-independent-loss tangent (flat tanδ) of their samples over a wide frequency spectrum (10^{-1}-10^{2} rad/s)[64]. Therefore, in order to investigate the deviation of neat PLA results from LST theory's proposed range of relaxation exponent ($0 \leq n < 1$), the effect of temperature on the phase angle was further explored. Fig. 14 demonstrates tanδ versus frequency of neat PLA at temperature spectrum of 150-200ºC. The results suggest that the loss tangent did not become independent of frequency; hence, the critical gel behaviour was not obtained over this temperature range. Therefore, the absence of the critical gel behaviour in the polymeric matrix could have been a main cause of obtaining exponent values larger than the proposed ones. Moreover, it has been shown that the presence of the strain hardening behaviour in extensional viscosity is only possible below T_{gel} of the polymeric systems (Sugimoto, et al. 2007).

In a study conducted by Liu et al. (2003), the gelation behaviour of polycarbonate-carbon nanotubes (PC/CNT) composites has been attributed to the entanglement of CNTs (caused by large aspect ratio and intrinsic random curvature of the defective nanotubes), as well as the non-covalent interaction between polymer chains and CNTs. The formation of the interconnecting structure of nano fillers occurred at the percolation threshold which resulted in the enhancement of storage modulus of their samples. They assigned this increase in G' to the hindrance of the straight forward relaxation of polymer chains as a result of the mutual constraint of the percolation threshold structure. They also showed that in polymer/CNT gels, the values of the gel point, gel strength (S) and relaxation exponent (n) are dependent on the level of dispersion of CNTs within polymeric matrix, the aspect ratio of CNTs and the interaction between CNTs and the polymer matrix [61]. Therefore, poor dispersion of NGP fillers within the polymeric matrix (morphological analysis section) could have also contributed to inadequate exhibition of gelation behaviours in PLA/NGP.

Overall, the emergence of the relaxation equilibrium and characteristic times of PLA05-PLA10 samples may support the occurrence of liquid-solid transition behaviour at about 3 wt% filler content composites, which is in conformance with the slope (α) analysis and the mechanical percolation threshold of this study. Moreover, poor demonstration of gelation behaviour of neat PLA and PLA/NGP samples is not consistent with the Liquid-solid transition theory proposed by Winter and Chambon. Two main causative factors behind this inconsistency could be the absence of T_{gel} within the testing temperature spectrum in addition to poor dispersion of nanofillers within PLA matrix. Further investigations of this discrepancy will be performed through extensional rheological analysis of the samples in an upcoming study.

4. Conclusion

PLA/NGP composites were prepared via melt intercalation mixing process. Results of the dynamic strain sweep tests showed that the composites with filler contents above 3 wt% exhibited pronounced nonlinear viscoelastic behaviour at strains greater than 2%. Through dynamic frequency sweep tests, the master curves of storage and loss moduli showed that the change in

liquid-like behaviour into pseudo-solid-like behaviour occurred at 3 wt% NGP content composites. The complex viscosity master curves illustrated a change from Newtonian to shear thinning behaviour at low frequency region occurred at 5 wt% filler content. The rheological percolation threshold of composites via investigation of slope (α) was found to be around 3 wt% NGP content. The validity of Cox-Merz relation was not satisfied in these composites and it failed at both low and high shear rates. The modelling of steady shear viscosity results revealed a transition of behaviour from 3-5 wt% nanofiller content. The presence of the characteristic time and relaxation equilibrium for samples with NGP filler contents beyond 3 wt% could be attributed to the manifestation of liquid-solid transition of the composites in that region. However, the composites and neat PLA demonstrated dissatisfactory gelation properties, the effects of which are yet to be investigated.

Most importantly, this study revealed that polylactide and nanographite platelets are appropriate options for the fabrication of biodegradable nanocomposites from a mere rheological standpoint. The interfacial compatibility between PLA chains and NGP fillers was exhibited through the successful application of steady (Carreau-Yasuda) and dynamic (time-temperature superposition, slope α percolation threshold analysis and Winter- Chambon liquid-solid transition theory) melt shear rheological modelling of the composites. Nonetheless, poor dispersion of NGP fillers within PLA matrix in conjunction with the application of a working temperature different from T_{gel} of the samples could have been the principal driving factors behind the observed discrepancies from the proposed gelation theory.

Furthermore, mechanical testing showed most improvement of Young's modulus at 3 wt% filler content sample. Morphological analysis of the samples suggested that adequate dispersion of nanofillers was not achieved in this study. Therefore, the PLA/NGP samples cannot be categorized as nanocomposites and in fact, it suggests that the dispersion of graphite platelet layers into PLA matrix may not be efficiently accomplished through melt intercalation and dry mixing process. Our future studies will focus on extensional rheological testing of the samples as well as the application of solvent-casting techniques, in order to improve the dispersion of NGP fillers in PLA matrix.

Acknowledgments

The authors would like to greatly appreciate the insightful and instructive advices received from Prof. Gareth H. McKinley (Massachusetts Institute of Technology) who made several valuable suggestions that have led to significant improvements of this manuscript.

Table Captions

Table 1. Compositions of PLA/NGP composites and their corresponding sample codes.

Table 2. Critical strain values of neat PLA and PLA/NGP composites. The values were estimated from the change in the slope of the moving average trendline of each individual curve.

Table 3. Slope (α**)** of G' and G" of samples at lower frequency region ($0.01 > \omega > 1$).

Table 4. Zero-shear viscosity, critical shear rate, and characteristic time of samples measured during steady shear sweep test at 180 ^{o} C.

Table 5. Carreau and Carreau-Yasuda model (equations 2 and 3) parameters of neat PLA and PLA/NGP systems.

Table 6. Gelation properties of neat PLA and PLA/NGP composites. Data were calculated utilizing equations 6, 9, 10 and 11.

Figure Captions

Fig1. Comparative XRD diffractograms of composites after compression moulding: 0-10% NGP content.

Fig2. TEM micrographs of PLA/NGP composites at 0.2 µm magnification microtomed from compression moulded specimens: PLA01 (a, b), PLA03(c, d), PLA05(e, f), PLA07(g, h), PLA10(i, j).

Fig3. Young's modulus and elongation at break of neat PLA and PLA/NGP composites as a function of NGP content.

Fig4. Evaluation of the linear viscoelastic response (logarithmic scales) of neat PLA and PLA/NGP composites at constant frequency.

Fig5. Comparative master curves of reduced frequency dependence of (a): storage modules (G') and (b): loss modules (G") versus frequency (bi-logarithmic scales) of neat PLA and PLA/NGP composites. Measurements conducted at 170, 180, 190, and 200^{O}C (T_{ref}= 180°C) and critical strain of samples over full range of frequency (0.01-100 rad.s^{-1}).

Fig6. Comparative master curves of Complex viscosity, |η*|, versus frequency (bi-logarithmic scales) of neat PLA and PLA/NGP composites. Measurements conducted at 170, 180, 190, and 200^{O}C (T_{ref}= 180°C) and critical strain of samples over full range of frequency (0.01-100 rad/s).

Fig7. Slope (α**)** of G' as a function of NGP content of the samples at lower frequency region (0.01> ω >1). The intersection in "moving average trendline" indicates the location of percolation threshold region.

Fig8. Steady shear viscosity as a function of shear rate (logarithmic scales) for neat PLA and PLA/NGP composites at 180^{o}C.

Fig9. Comparison between steady shear viscosity versus generalized models of selected (neat PLA and PLA07) systems as a function of shear rate at 180^{o}C.

Fig10. The loss tangent (tan δ) of the samples at different frequencies, as a function of NGP filler contents of PLA/NGP composites.

Fig11. G' (solid) and G''/tan (nπ/2) (dashed) of PLA/NGP composites at different frequencies versus their corresponding NGP filler contents.

Fig12. Relaxation modulus of neat PLA and PLA/NGP composites against relaxation time (time of cross-linking) at 180^{o}C.

Fig13. Demonstration of the power law regions of the samples and their corresponding Winter-Chambon equation (equation 4) from Relaxation modulus versus relaxation time data (Temp. =180^{o}C).

Fig14. Demonstration of loss tangent (tanδ) of neat PLA versus angular frequency (ω) at temperature range 150-200°C.

References

1. A. Khare and S. Deshmukh, *Journal of Plastic Film and Sheeting,* **22**, 3 (2006).
2. M. Darder, P. Aranda, and E. Ruiz-Hitzky, *Advanced Materials,* **19**, 10 (2007).
3. S. Sinha Ray, K. Yamada, M. Okamoto, and K. Ueda, *Polymer,* **44**, 3 (2003).
4. Q. Fang and M.A. Hanna, *Industrial Crops and Products,* **10**, 1 (1999).
5. N. Ogata, G. Jimenez, H. Kawai, and T. Ogihara, *Journal of Polymer Science, Part B: Polymer Physics,* **35**, 2 (1997).
6. K. Fukushima, M. Murariu, G. Camino, and P. Dubois, *Polymer Degradation and Stability,* **95**, 6 (2010).
7. A.M. Harris and E.C. Lee, *Journal of Applied Polymer Science,* **107**, 4 (2008).
8. P. Dubois and M. Murariu, *JEC Composites Magazine,* **45**, 45 (2008).
9. S. Solarski, M. Ferreira, E. Devaux, G. Fontaine, P. Bachelet, S. Bourbigot, R. Delobel, P. Coszach, M. Murariu, A. Da Silva Ferreira, M. Alexandre, P. Degee, and P. Dubois, *Journal of Applied Polymer Science,* **109**, 2 (2008).
10. S. Sinha Ray and M. Okamoto, *Macromolecular Rapid Communications,* **24**, 14 (2003).
11. P. Maiti, K. Yamada, M. Okamoto, K. Ueda, and K. Okamoto, *Chemistry of Materials,* **14**, 11 (2002).
12. T. Villmow, P. Pötschke, S. Pegel, L. Häussler, and B. Kretzschmar, *Polymer,* **49**, 16 (2008).
13. M.A. Paul, C. Delcourt, M. Alexandre, P. Degée, F. Monteverde, A. Rulmont, and P. Dubois, *Macromolecular Chemistry and Physics,* **206**, 4 (2005).
14. Y. Zhu, S. Murali, W. Cai, X. Li, J.W. Suk, J.R. Potts, and R.S. Ruoff, *Advanced Materials,* **22**, 35 (2010).
15. A.K. Geim and K.S. Novoselov, *Nature Materials,* **6**, 3 (2007).
16. O.C. Compton and S.T. Nguyen, *Small,* **6**, 6 (2010).
17. J.R. Potts, D.R. Dreyer, C.W. Bielawski, and R.S. Ruoff, *Polymer,* **52**, 1 (2011).
18. S. Park and R.S. Ruoff, *Nature nanotechnology,* **4**, 4 (2009).
19. A. Dato, V. Radmilovic, Z. Lee, J. Phillips, and M. Frenklach, *Nano Letters,* **8**, 7 (2008).
20. B.Z. Jang and A. Zhamu, *Journal of Materials Science,* **43**, 15 (2008).
21. G. Chen, D. Wu, W. Weng, and C. Wu, *Carbon,* **41**, 3 (2003).
22. X.S. Du, M. Xiao, Y.Z. Meng, and A.S. Hay, *Polymer.,* **45**, (2004).
23. W. Zheng, X. Lu, and S.C. Wong, *Journal of Applied Polymer Science,* **91**, 5 (2004).
24. K. Kalaitzidou, H. Fukushima, P. Askeland, and L.T. Drzal, *Journal of Materials Science,* **43**, 8 (2008).
25. E. Narimissa, R. Gupta, M. Bhaskaran, and S. Sriram, *Polymer Degradation and Stability,* **97**, 5 (2012).
26. E. Narimissa, R.K. Gupta, H.J. Choi, N. Kao, and M. Jollands, *Polymer Composites,* **33**, 9 (2012).
27. E. Narimissa, M. Jollands, N. Kao, and R. Gupta, Mechanical and thermal characterisation of biopolymer nanocomposites based on PLA/Nanographene platelets in 27th Annual Meeting of The Polymer Processing Society (PPS27), A.Q. R. Bouhfid, K. Benmoussa. B. Drissi. M. Bakkoury and M. Bousmina Editor 2011: Morocco p. 1-8.
28. S. Sinha Ray and M. Okamoto, *Macromolecular Materials and Engineering,* **288**, 12 (2003).
29. H. Fukushima and L.T. Drzal, *Annu. Tech. Conf. Soc. Plast. Eng.,* **61**, (2003).
30. A. Yasmin, J.J. Luo, and I.M. Daniel, *Composites Science and Technology,* **66**, 9 (2006).
31. M. Pluta, *Polymer,* **45**, 24 (2004).
32. H. Kim and C.W. Macosko, *Polymer,* **50**, 15 (2009).
33. P. Maiti and M. Okamoto, *Macromolecular Materials and Engineering,* **288**, 5 (2003).
34. V. Pasanovic-Zujo, R.K. Gupta, and S.N. Bhattacharya, *Rheologica Acta,* **43**, 2 (2004).
35. C. Thellen, C. Orroth, D. Froio, D. Ziegler, J. Lucciarini, R. Farrell, N.A. D'Souza, and J.A. Ratto, *Polymer,* **46**, (2005).
36. J. Kalfus and J. Jancar, *Polymer Composites,* **28**, 6 (2007).

37. A. Bhatia, Experimental study of structure and properties biodegradable nanocomposites, in School of civil, environmental and chemical engineering2008, RMIT: Melbourne. p. 171.
38. L.A. Utracki, *Polymer Alloys and Blends: Thermodynamics and Rheology*, Hanser Publishers, New York (1990).
39. J.D. Ferry, *Viscoelastic Properties of Polymers*, John Wiley and Sons, New York (1980).
40. S. Sinha Ray, K. Okamoto, and M. Okamoto, *Macromolecules,* **36**, 7 (2003).
41. M. Okamoto, P.H. Nam, P. Maiti, T. Kotaka, N. Hasegawa, and A. Usuki, *Nano Letters,* **1**, 6 (2001).
42. S. Sinha Ray, M. Bousmina, and K. Okamoto, *Macromolecular Materials and Engineering,* **290**, 8 (2005).
43. J.M. Dealy and D. Plazek, *Rheology Bulletin,* **78**, 2 (2009).
44. N.J. Distefano and K.S. Pister, *Acta Mechanica,* **13**, 3-4 (1972).
45. S.N. Bhattacharya, R.K. Gupta, and M.R. Kamal, *Polymeric Nanocomposites: Theory and Practice*, Hanser Gardner Pubns, Munich (2007).
46. A.K. Lau, F. Hussain, and K. Lafdi, eds. *Nano- and Biocomposites*. 2010, Taylor and Francis Group, LLC: Florida.
47. M.A. Treece and J.P. Oberhauser, *Polymer,* **48**, 4 (2007).
48. D.H. Kim, P.D. Fasulo, W.R. Rodgers, and D.R. Paul, *Polymer,* **48**, 18 (2007).
49. H.J. Choi, S.G. Kim, Y.H. Hyun, and M.S. Jhon, *Macromolecular Rapid Communications,* **22**, 5 (2001).
50. A. Subbotin, A. Semenov, E. Manias, G. Hadziioannou, and G. Ten Brinke, *Macromolecules,* **28**, 5 (1995).
51. S. Granick, *Materials Research Society Bulletin,* **21**, (1996).
52. R. Krishnamoorti, J. Ren, and A.S. Silva, *Chem. Phys.,* **114**, (2001).
53. G. Galgali, C. Ramesh, and A. Lele, *Macromolecules,* **34**, 4 (2001).
54. P.J. Carreau, D.C.R. De Kee, and R.P. Chhabra, *Rheology of Polymeric Systems*, Carl Hanser Verlag GmbH & Co New York (1997).
55. W.P. Cox and E.H. Merz, *Journal of Polymer Science,* **28**, 118 (1958).
56. R. Krishnamoorti, R.A. Vaia, and E.P. Giannelis, *Chemistry of Materials,* **8**, 8 (1996).
57. Y.H. Hyun, S.T. Lim, H.J. Choi, and M.S. John, *Macromolecules,* **34**, 23 (2001).
58. F. Chambon and H.H. Winter, *Polymer Bulletin,* **13**, 6 (1985).
59. H.H. Winter, *Polym. Eng. Sci.,* **27**, 22 (1987).
60. H.H. Winter, *Progress in Colloid & Polymer Science,* **75**, 1 (1987).
61. C. Liu, J. Zhang, J. He, and G. Hu, *Polymer,* **44**, 24 (2003).
62. H.H. Winter and M. Mours, *Adv. Polym. Sci.,* **134**, (1997).
63. J.M. Dealy and R.G. Larson, *Structure and Rheology of Molten Polymers: From Structure to Flow Behaviour and Back Again*, Hnaser, Munich (2006).
64. M. Sugimoto, H. Hida, T. Taniguchi, K. Koyama, and Y. Aoki, *Rheologica Acta,* **46**, 7 (2007).

TABLES

Table 1. Compositions of PLA/NGP composites and their corresponding sample codes.

	Sample Code					
Sample Compositions	**neat PLA**	**PLA01**	**PLA03**	**PLA05**	**PLA07**	**PLA10**
PLA content (wt%)	100	99	97	95	93	90
NGP content (wt%)	0	1	3	5	7	10
Times extruded (no.)	1	1	1	1	1	1

Table 2. Critical strain values of neat PLA and PLA/NGP composites. The values were estimated from the change in the slope of the moving average trendline of each individual curve.

Samples	Critical Strain (%)
neat PLA	100
PLA01	100
PLA03	25
PLA05	2.5
PLA07	0.2
PLA10	0.16

Table 3. Slope (α) of G' and G" of samples at lower frequency region (0.01> ω >1).

Samples	Slope (α) G'	Slope (α) G"
neat PLA	1.9	1.7
PLA01	1.8	1.6
PLA03	1.4	1.4
PLA05	0.7	1.3
PLA07	0.3	1
PLA10	0	0.1

Table 4. Zero-shear viscosity, critical shear rate, and characteristic time of samples measured during steady shear sweep test at 180 ^{o} C.

Samples	η_0 (Pa.s)	CSR (S^{-1})	λ (s)
neat PLA	1250	2.00	0.50
PLA01	1290	1.58	0.65
PLA03	1600	0.08	12.60
PLA05	2060	0.06	15.85
PLA07	2650	0.02	25.15
PLA10	3980	0.015	39.80

Table 5. Carreau and Carreau-Yasuda model (equations 2 and 3) parameters of neat PLA and PLA/NGP systems.

Sample	zero-η (Pa.S)	Carreau Model		Carreau-Yasudu Model		
		λ (s)	n	λ (s)	n	a
neat PLA	1250	0.30	0.00	0.35	0.00	4.95
PLA01	1290	0.40	0.00	0.45	0.00	4.95
PLA03	1600	0.75	0.00	0.40	0.00	1.10
PLA05	2060	22.50	0.90	11.40	0.85	1.00
PLA07	2650	27.55	0.70	28.20	0.70	2.20
PLA10	3980	29.00	0.85	31.00	0.80	3.45

Table 6. Gelation properties of neat PLA and PLA/NGP composites. Data were calculated utilizing equations 6, 9, 10 and 11.

	Sample Code					
	neat PLA	PLA01	PLA03	PLA05	PLA07	PLA10
$G_{e\ (Pa)}$	0	0	0	1.27	0.40	25.95
λ_{max} (s)	0	0	0	1.96	1.37	0.50
Γ(n)	1.72	2.16	1.47	1.10	1.27	1.21
S (Pa s^n)	0.82	0.38	1.96	5.56	0.86	5.11
n	2.83	3.08	2.63	2.20	2.43	2.36

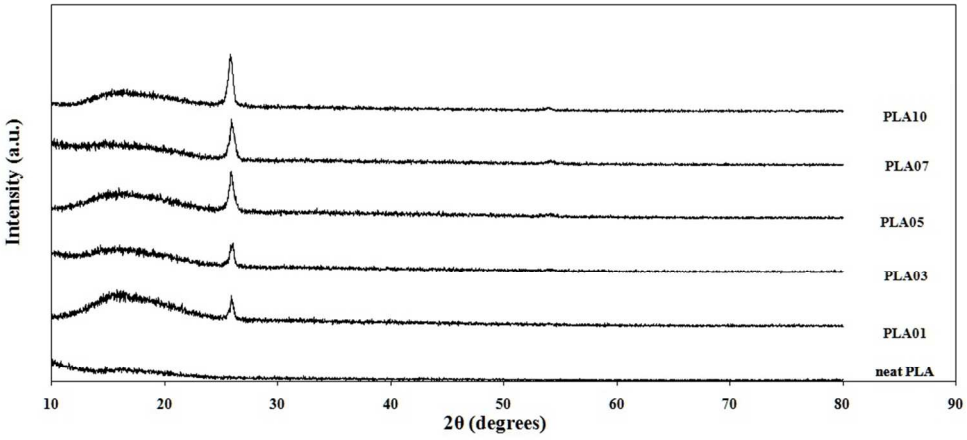

Fig1. Comparative XRD diffractograms of composites after compression moulding: 0-10% NGP content.
183x86mm (144 x 144 DPI)

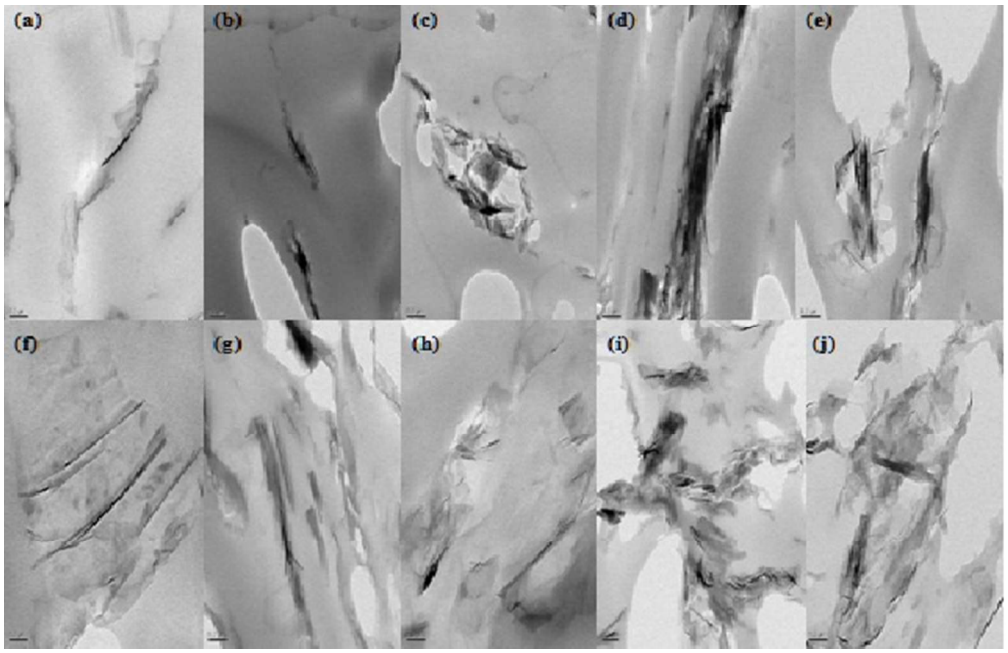

Fig2. TEM micrographs of PLA/NGP composites at 0.2 μm magnification microtomed from compression moulded specimens: PLA01 (a, b), PLA03(c, d), PLA05(e, f), PLA07(g, h), PLA10(i, j).
112x72mm (144 x 144 DPI)

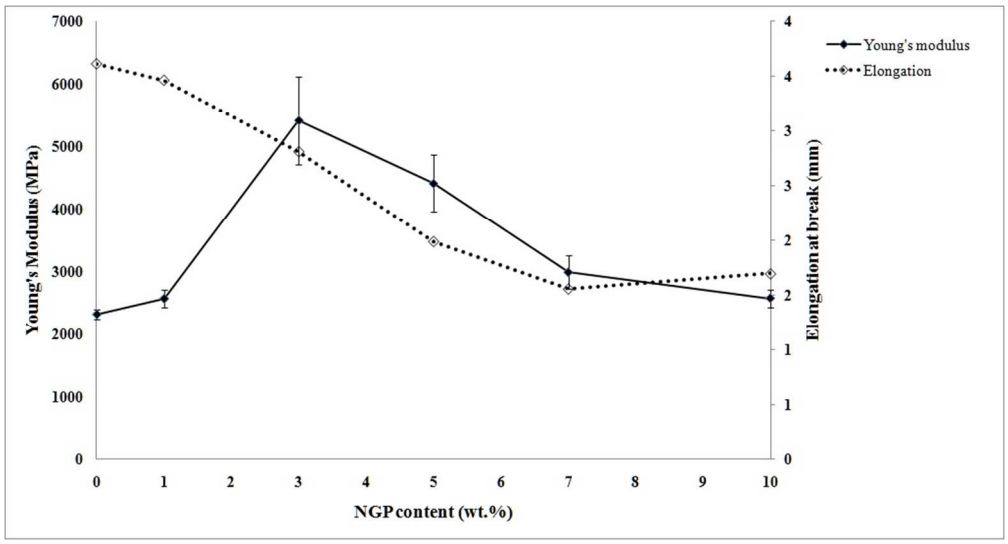

Fig3. Young's modulus and elongation at break of neat PLA and PLA/NGP composites as a function of NGP content.
180x96mm (144 x 144 DPI)

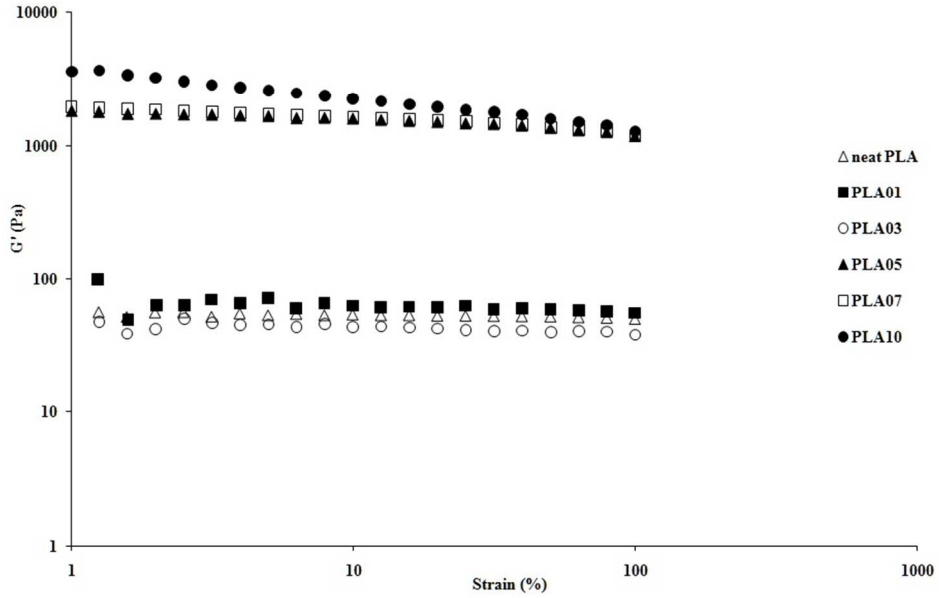

Fig4. Evaluation of the linear viscoelastic response (logarithmic scales) of neat PLA and PLA/NGP composites at constant frequency.
170x104mm (144 x 144 DPI)

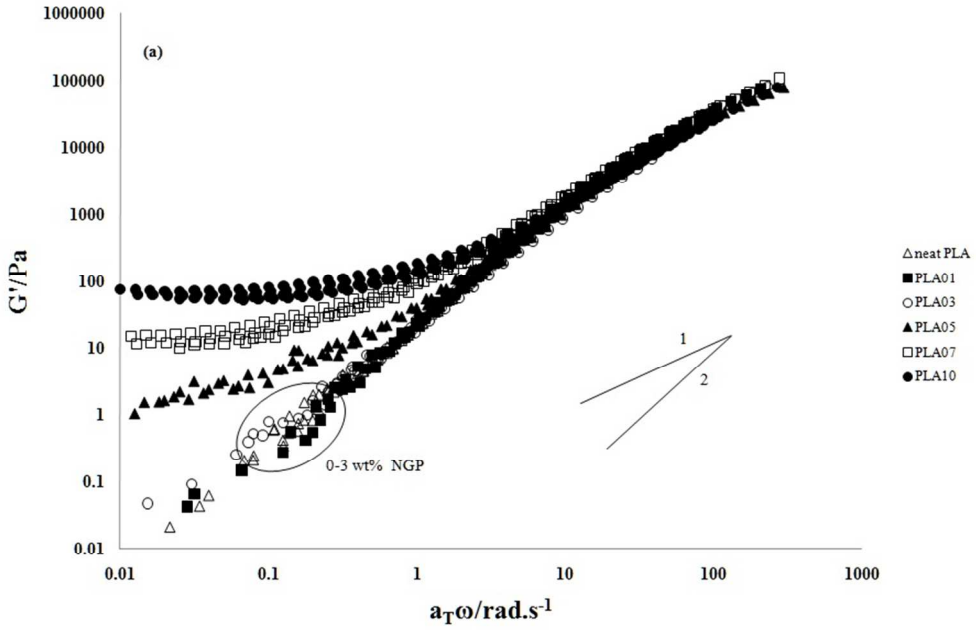

Fig5. Comparative master curves of reduced frequency dependence of (a): storage modules (G') and (b): loss modules (G") versus frequency (bi-logarithmic scales) of neat PLA and PLA/NGP composites. Measurements conducted at 170, 180, 190, and 200OC (Tref= 180°C) and critical strain of samples over full range of frequency (0.01-100 rad.s-1).
160x104mm (144 x 144 DPI)

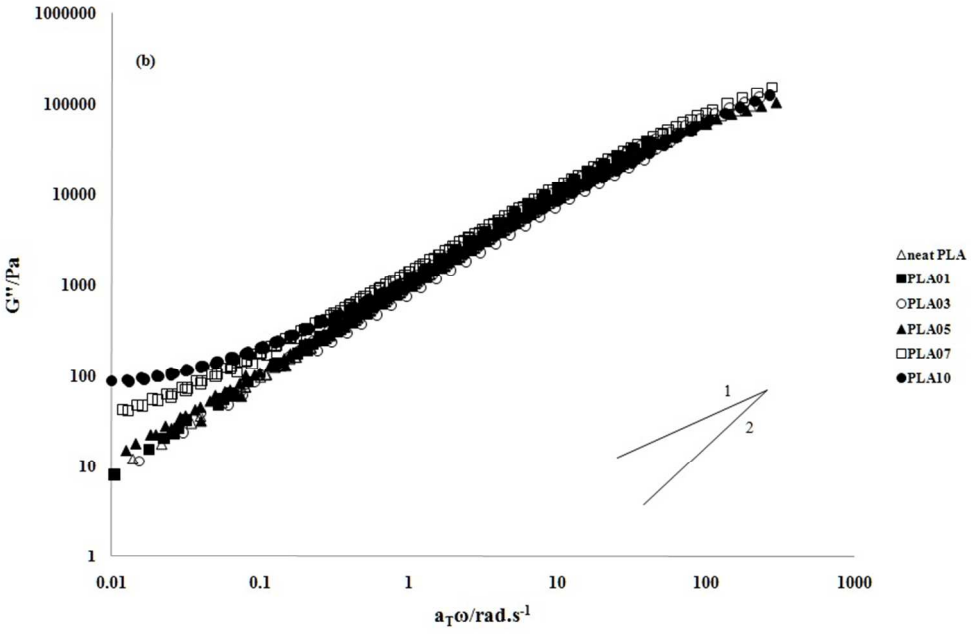

Fig5. Comparative master curves of reduced frequency dependence of (a): storage modules (G') and (b): loss modules (G") versus frequency (bi-logarithmic scales) of neat PLA and PLA/NGP composites. Measurements conducted at 170, 180, 190, and 200OC (Tref= 180°C) and critical strain of samples over full range of frequency (0.01-100 rad.s-1).
160x104mm (144 x 144 DPI)

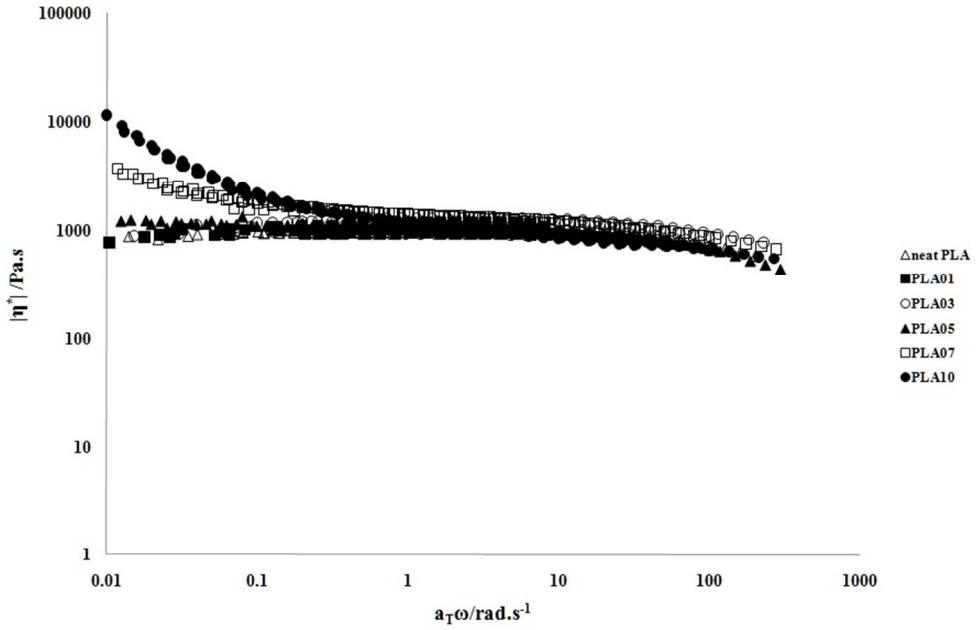

Fig6. Comparative master curves of Complex viscosity, |η*|, versus frequency (bi-logarithmic scales) of neat PLA and PLA/NGP composites. Measurements conducted at 170, 180, 190, and 200OC (Tref= 180°C) and critical strain of samples over full range of frequency (0.01-100 rad/s).
160x104mm (144 x 144 DPI)

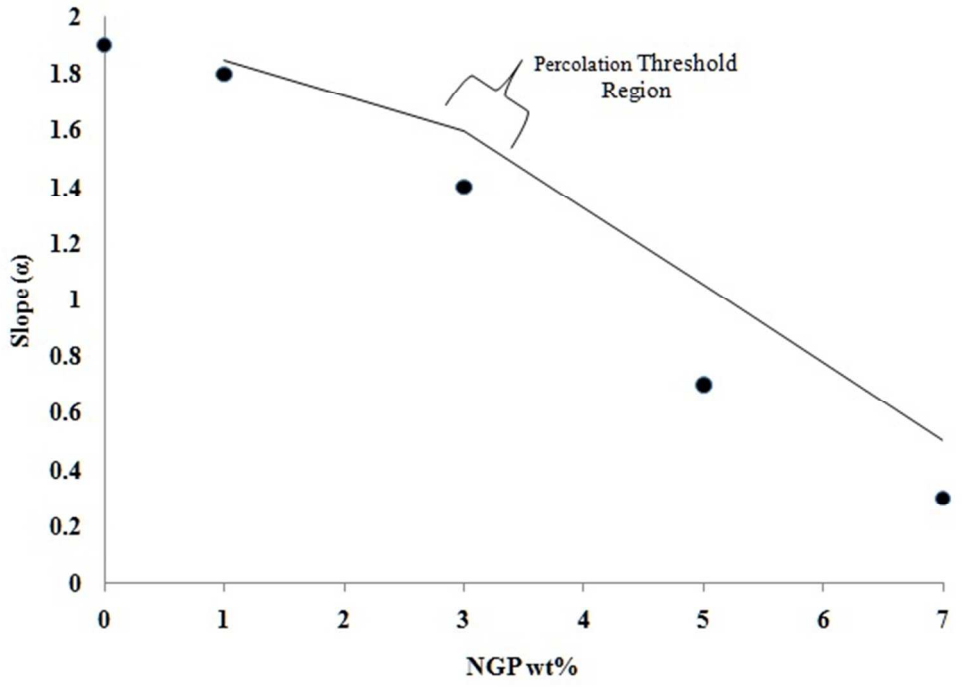

Fig7. Slope (α) of G' as a function of NGP content of the samples at lower frequency region (0.01> ω >1). The intersection in "moving average trendline" indicates the location of percolation threshold region.
109x78mm (144 x 144 DPI)

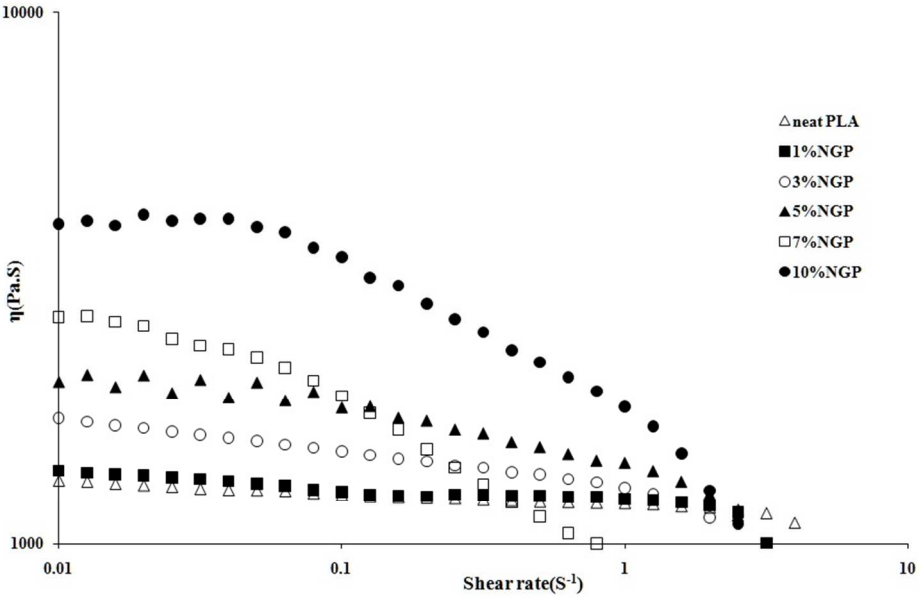

Fig8. Steady shear viscosity as a function of shear rate (logarithmic scales) for neat PLA and PLA/NGP composites at 180oC.
170x104mm (144 x 144 DPI)

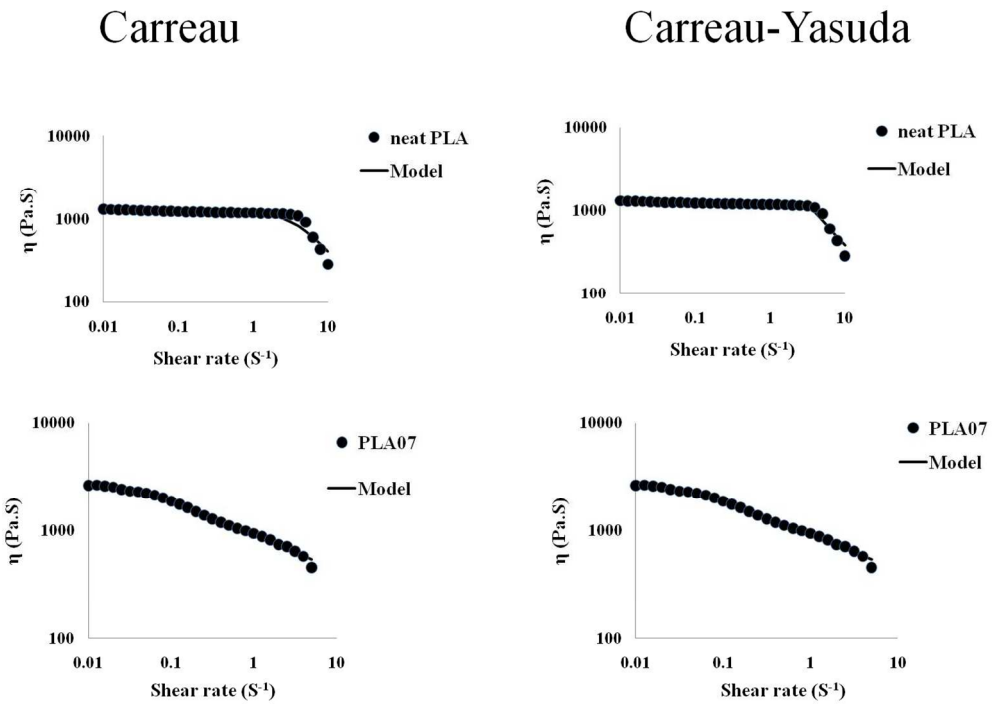

Fig9. Comparison between steady shear viscosity versus generalized models of selected (neat PLA and PLA07) systems as a function of shear rate at 180oC.
264x190mm (144 x 144 DPI)

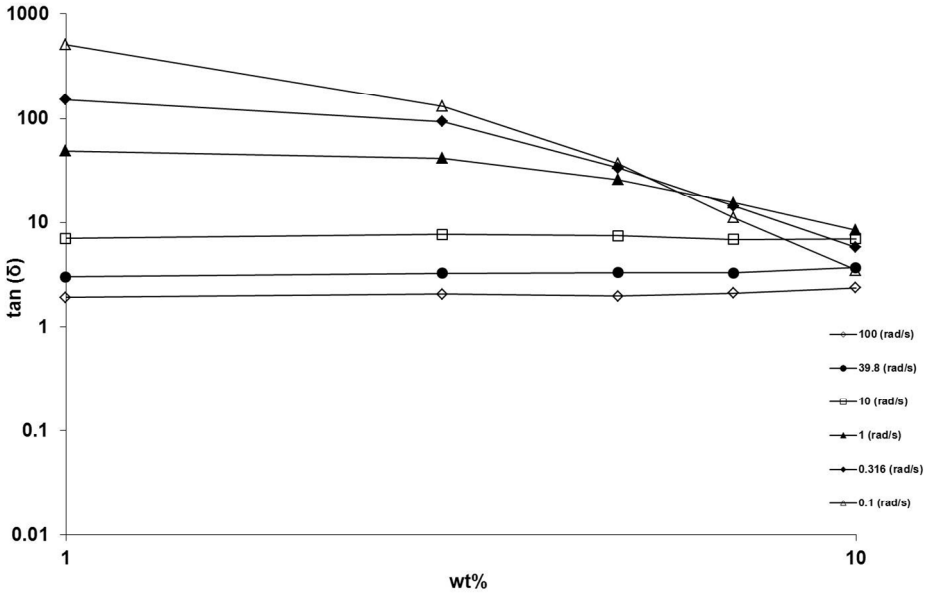

Fig10. The loss tangent (tan δ) of the samples at different frequencies, as a function of NGP filler contents of PLA/NGP composites.
266x162mm (144 x 144 DPI)

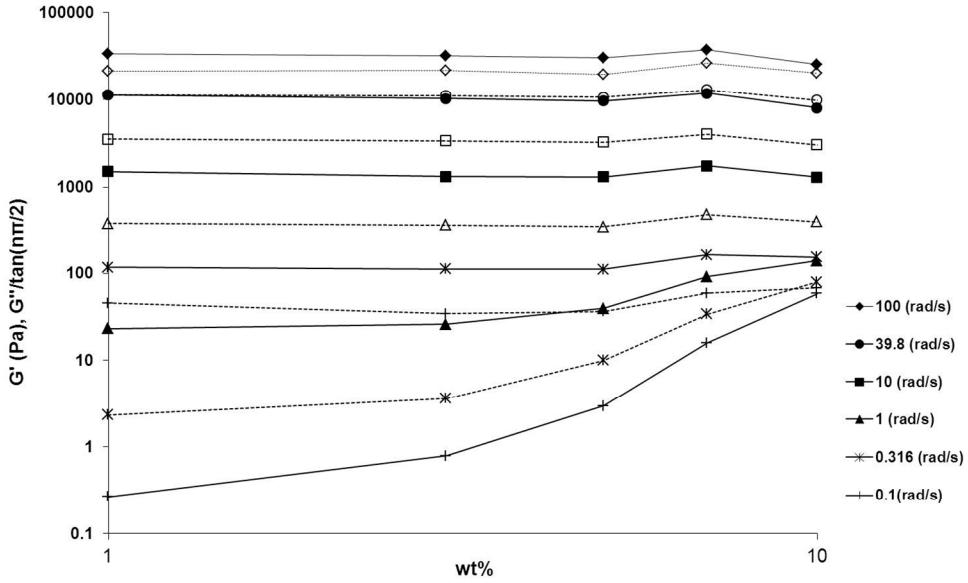

Fig11. G' (solid) and G''/tan (nΠ/2) (dashed) of PLA/NGP composites at different frequencies versus their corresponding NGP filler contents.
266x162mm (144 x 144 DPI)

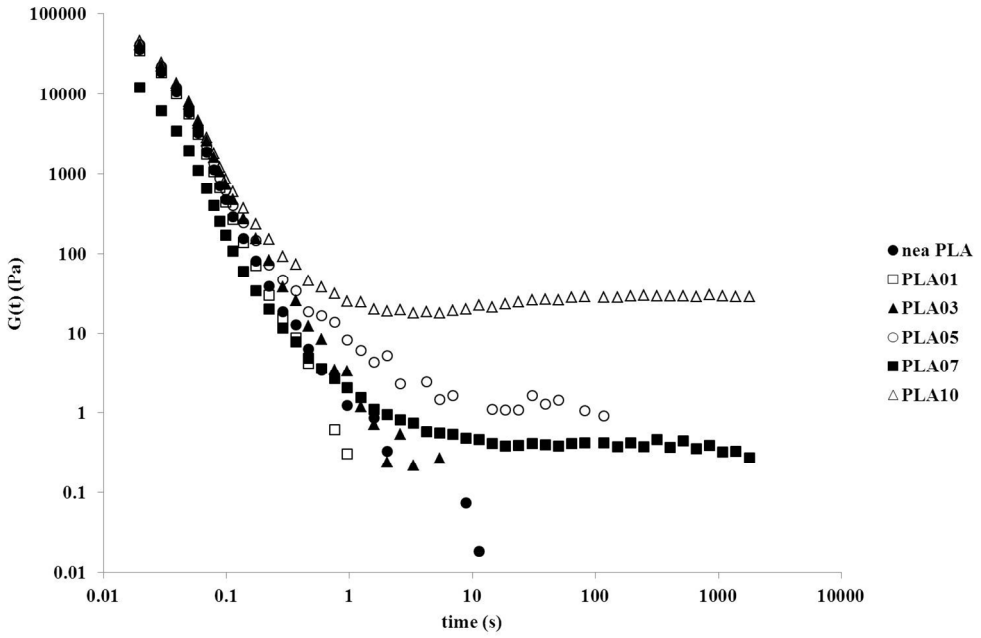

Fig12. Relaxation modulus of neat PLA and PLA/NGP composites against relaxation time (time of cross-linking) at 180oC.
269x175mm (144 x 144 DPI)

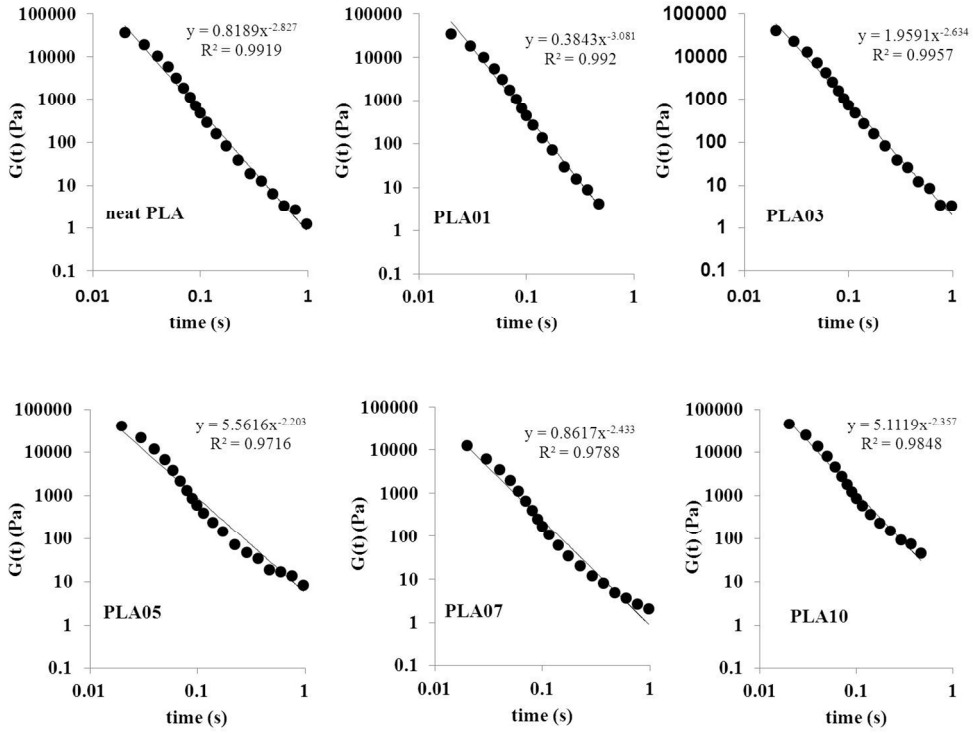

Fig13. Demonstration of the power law regions of the samples and their corresponding Winter-Chambon equation (equation 4) from Relaxation modulus versus relaxation time data (Temp. =180oC).
265x198mm (144 x 144 DPI)

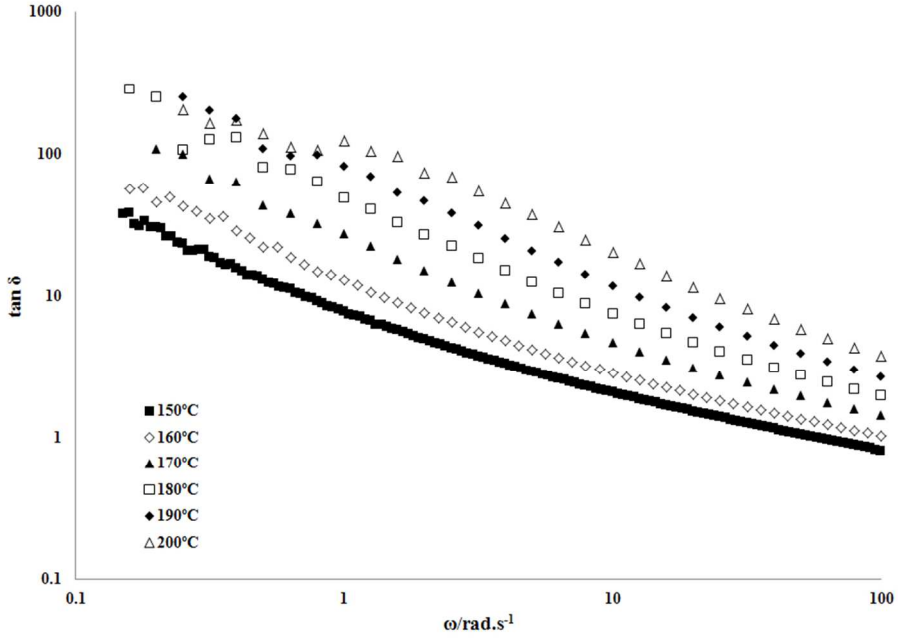

Fig14. Demonstration of loss tangent (tanδ) of neat PLA versus angular frequency (ω) at temperature range 150-200°C.
172x112mm (144 x 144 DPI)

Melt Rheological Investigation of Polylactide-Nanographite Platelets Biopolymer Composites

Esmaeil Narimissa,[1] Rahul K. Gupta,[1] Nhol Kao,[1] Hyoung J. Choi,[2] Margaret Jollands,[1] Sati N. Bhattacharya[1]

[1] *Rheology and Materials Processing Centre (RMPC), School of Civil, Environmental and Chemical Engineering, RMIT University, Melbourne, Victoria 3000, Australia*

[2] *Department of Polymer Science and Engineering, Inha University, Incheon 402-751, Korea*

This study is an analytical investigation of processability of biopolymer-carbon based nanofiller composites primarily through rheological investigation of samples. The composites were fabricated via dry mixing and melt-blending of biodegradable polylactide (PLA) and nanographite platelets (NGP) in a Brabender twin screw extruder. A range of different nanofiller contents (1, 3, 5, 7, and 10 wt %) were studied for NGP containing composites. The morphology was studied with X-ray diffraction and transmission electron microscopy techniques and showed poor dispersion, with agglomerates, tactoids, and exfoliated layers present. Mechanical properties showed an optimum at 3 wt % filler. Results showed that the composites exhibited higher elastic and viscous moduli than neat PLA. The rheological percolation threshold predicted by changes in slope (α) as well as liquid–solid transition theory of samples was found around 3 wt % through the change from liquid-like behavior to pseudo-solid-like behavior at terminal region during dynamic oscillatory measurements. NGP nanofillers were found to enhance the viscoelastic and mechanical properties of PLA at low concentrations; however, an efficient dispersion of nanofillers within polymer by melt intercalation method of mixing was not achieved. POLYM. ENG. SCI., 00:000–000, 2013. © 2013 Society of Plastics Engineers

INTRODUCTION

In the production of bioplastics, biodegradable natural polymers extracted from renewable resources such as polylactide (PLA), polycaprolactone (PCL), cellulose, and starch are considered a more suitable alternative than petroleum-derived synthetic plastics. The degradation of these polymers by microorganisms generates nontoxic components in the environment reducing world-wide dependence on fossil fuels [1, 2]. Disposal of nonbiodegradable polymers and their composites through incineration on the other hand, may produce toxic gases and contribute to global pollution [3]. Research in the field of bionanocomposites can contribute to the efficiency of recycling waste management and green house emissions. The Benign properties of PLA toward the environment and its production from renewable resources make it a strong candidate as a substitute for petroleum based polymers.

PLA is a biodegradable thermoplastic polyester with linear aliphatic monomers, polymerized from lactic acid derived from fermentation of cornstarch [2]. Despite a number of PLA's promising properties (i.e., biocompatibility, thermal plasticity, and mechanical properties) it has failed to show similar satisfactory outcomes in its gas barrier properties, impact factor, and heat distortion temperature in different applications [4, 5]. Insufficient thermal, mechanical, barrier, and flame retardant properties of PLA have limited its application [6]. For example, automotive industry applications require material properties, where PLA grades are deficient in high durability, tight tolerances and efficient impact performance. The control of crystallinity of PLA through the addition of nanosized particles could lead to improvements in PLA properties such as heat deflection temperature, overall strength, chemical resistance, and stiffness [7]. The most popular nano-reinforcement in PLA studies to date is layered-silicate clay. This is due to the nanofiller's low cost, availability, and satisfactory enhancements brought into mechanical, barrier, and thermal properties of neat PLA, in addition to its acting as a nucleating agent to improve the crystallinity of PLA [8, 9].

Melt intercalation is the main process for fabrication of PLA bionanocomposites, due to its simplicity and economic viability [10, 11]. This process has been shown to produce interrelated nanocomposites with improved

Correspondence to: Rahul K. Gupta; e-mail: rahul.gupta@rmit.edu.au
DOI 10.1002/pen.23550
Published online in Wiley Online Library (wileyonlinelibrary.com).

properties such as stiffness, thermal stability, fire retardancy, and lower barrier permeability [9, 12]. Exfoliation of nanofillers in PLA nanocomposites has been demonstrated via *in situ* polymerization of lactic acid monomers as well as solvent-casting technique [13].

Graphene is a monolayer of sp^2-hybridized carbon atoms arranged in a two-dimensional lattice, which has been studied extensively due to its extraordinary thermal, mechanical and electrical properties [14–16]. Nanocomposites have been amongst the most promising areas of application of graphene-based compounds [17]. Micromechanical exfoliation of graphite, growth by chemical vapor deposition, and growth on crystalline silicon carbide are the main approaches to producing defect free pristine graphene with exceptional physical properties [14, 18]. However, these techniques do not produce sufficient quantities of graphene required for industrial-scale fabrication of nanocomposites [19]. Thus, producing nanocomposites using graphene-based compounds through the precursors of graphene (such as graphite oxide (GO) and nanographite platelets (NGPs) is a suitable alternative method [17].

Intercalation of graphite by a mixture of nitric and sulfuric acid can produce higher stage graphite-intercalated compounds (GIC) that can be exfoliated via microwave treatment or rapid heating of dried down generating expanded graphite (EG) [20, 21]. GICs and GOs can be subsequently utilized as precursor materials to produce scalable NGPs (monolayer carbon sheets or few-layer platelets with heteroatoms). NGPs contain a platelet structure and low price of clay, possess electrical and thermal properties of carbon nanotubes (CNTs) and have the potential to improve the crystallization behavior of PLA. Furthermore, due to their length and thickness, the entanglement of CNTs and carbon nanofibres (CNFs) are compatible with NGPs, which may contribute in the reduction of agglomeration. In addition, the electrical conductivity of NGPs is close to the electrical conductivity of copper, while also having a quarter of its density and fifty times higher mechanical strength than steel [22, 23]. In terms of crystallization, research has shown that NGPs can induce the nucleation of β-form crystals in polypropylene (PP), which are superior to α-form [24].

The main objective of this study was to investigate the interfacial compatibility and interactions between PLA chains and NGPs for the purpose of fabricating biodegradable PLA/NGP nanocomposites via dry mixing and melt-blending processes. To achieve this goal, melt rheological characterization of the samples was followed by the modeling of the results through utilization of eminent mathematical steady and dynamic rheological models of viscoelasticity. The steady shear rheology of the samples was investigated by means of Carreau-Yasuda model as well as the application of Cox-Merz relation while time–temperature superposition and slope α analysis of the percolation threshold were applied to study the dynamic shear rheological behaviors of samples. In addition, a comprehensive investigation based on liquid–solid transition (LST) theory, proposed by Winter and Chambon (1986), was also carried out to study the percolation threshold and gelation properties of the composites. Furthermore, the authors have already performed detailed investigations of the thermal, morphological, and mechanical properties of the samples [25–27].

TABLE 1. Compositions of PLA/NGP composites and their corresponding sample codes.

Sample compositions	Sample code					
	Neat PLA	PLA01	PLA03	PLA05	PLA07	PLA10
PLA content (wt %)	100	99	97	95	93	90
NGP content (wt %)	0	1	3	5	7	10
Times extruded (no.)	1	1	1	1	1	1

EXPERIMENTAL

Materials

Poly (L,L-lactide)-(PLA) was supplied by NatureWorks LLC and the grade of PLA used was 3051D with melt index and specific gravity of 10–30 g/10 min and 1.24, respectively. NGPs were supplied by XG Sciences, US Michigan and the grade of NGP used for this study was "M" with characteristics: average thickness of approximately 6–8 nm and a typical surface area of 120–150 m^2/g. According to the material data sheet, Grade M (xGnp-M) is available with average particle diameters of 5, 15, or 25 μm.

Processing

Drying of PLA to less than 250 ppm is a necessary first step before the processing phase. Thus, PLA pellets used in this study were first dried in a fan dryer at a temperature of 50°C for 7 days earlier than the melt-blending process.

PLA pellets and NGP were dry mixed in the desired composition before melt blending in 700 g batches. Table 1 shows the compositions (nominal wt %) and the codes of neat PLA and PLA/NGP samples (hereafter, samples are referred to according to their sample codes).

Samples were melt-blended in a Brabender Twin Screw extruder. The speed and temperature of the extruder were set at 180°C and 40 RPM, as too high or too low extrusion temperatures or speed may result in thermal degradation and/or insufficient shear for proper mixing of nanocomposites. Subsequently, the extruded composites were pelletized and then stored in a vacuum oven at 50°C before further processing.

Dried pellets were compression molded into 2-mm-thick circular plaque with 20-mm diameter specimens.

DOI 10.1002/pen